

THE SAGITTARIUS STREAMS IN THE SOUTHERN GALACTIC HEMISPHERE

SERGEY E. KOPOSOV^{1,2}, V. BELOKUROV¹, N.W. EVANS¹, G. GILMORE¹, M. GIELES¹, M.J. IRWIN¹, G.F. LEWIS^{1,3}, M. NIEDERSTE-OSTHOLT¹, J. PEÑARRUBIA¹, M.C. SMITH⁴, D. BIZYAEV^{5,2}, E. MALANUSHENKO⁵, V. MALANUSHENKO⁵, D.P. SCHNEIDER⁶, R.F.G. WYSE⁷

Draft version July 6, 2018

ABSTRACT

The structure of the Sagittarius stream in the Southern Galactic hemisphere is analysed with the Sloan Digital Sky Survey Data Release 8. Parallel to the Sagittarius tidal track, but $\sim 10^\circ$ away, there is another fainter and more metal-poor stream. We provide evidence that the two streams follow similar distance gradients but have distinct morphological properties and stellar populations. The brighter stream is broader, contains more metal-rich stars and has a richer colour-magnitude diagram with multiple turn-offs and a prominent red clump as compared to the fainter stream. Based on the structural properties and the stellar population mix, the stream configuration is similar to the Northern “bifurcation”. In the region of the South Galactic Cap, there is overlapping tidal debris from the Cetus Stream, which crosses the Sagittarius stream. Using both photometric and spectroscopic data, we show that the blue straggler population belongs mainly to Sagittarius and the blue horizontal branch stars belong mainly to the Cetus stream in this confused location in the halo.

Subject headings: galaxies: dwarf – galaxies: individual (Sagittarius) – Local Group

1. INTRODUCTION

The Milky Way has clearly not finished assembling, as the two Magellanic Clouds are coalescing into the Galaxy. As stochastic satellite infall continues in the Galactic halo, it gives us a chance to bootstrap our cosmological theories of structure formation to the local observables. By measuring the signatures of accretion of galactic fragments – manifested in streams of stripped gas and stars – onto the Milky Way, we can study the Galaxy’s underlying matter distribution.

Of the Galactic satellites surviving to date, the Sagittarius (Sgr) dwarf galaxy is one of the most massive, third after the LMC and SMC (e.g. Niederste-Ostholt et al. 2010). It is however, not going to survive for much longer. After its discovery by Ibata et al. (1994), it was quickly realized that the Sgr dwarf was losing its stars to the Galactic tides at a high rate (e.g. Johnston et al. 1995; Lynden-Bell & Lynden-Bell 1995; Mateo et al. 1996). It was only when most of the sky was imaged by the 2MASS and the SDSS surveys that the amount of damage done to Sgr became really apparent (e.g. Newberg et al. 2002; Majewski et al. 2003). Currently, it is established that the stellar debris torn from the dwarf wraps around the Galaxy at least once, i.e. leading and trailing tails can be each seen covering over π radians on

the sky (Majewski et al. 2003; Belokurov et al. 2006). Hundreds of stars in the Sgr tails have their radial velocities measured and some of these also have reliable chemical abundances (Majewski et al. 2004; Chou et al. 2007; Monaco et al. 2007; Yanny et al. 2009; Chou et al. 2010). A number of star clusters are believed to have originated in Sgr and are now left free-floating in the Milky Way halo after having been torn from the disrupting galaxy (e.g. Law & Majewski 2010b).

Unfortunately, the unbound stars (and star clusters) are not simply tagged according to their past Sgr membership. Instead, objects are typically classified as such based on their proximity to the Sgr orbital plane, their heliocentric distances and radial velocities. Models have had some considerable success explaining this data (e.g. Law & Majewski 2010a), but difficulties remain. In particular, the Virgo Over-density (Jurić et al. 2008) and the “bifurcation” of the leading tail (Belokurov et al. 2006) are both examples of substructures that lie close to the Sgr plane whose origins remain obscure. Although there were attempts to include these in the picture of Sgr disruption (e.g. Fellhauer et al. 2006; Martínez-Delgado et al. 2007; Peñarrubia et al. 2010), it now seems that little progress has been made.

Finally, another stream (the Cetus stream) on a polar orbit has recently been announced to overlap with Sgr debris in the Southern Galactic hemisphere by Newberg et al. (2009). Although this has a different kinematical signature to Sgr, it coincides in space and metallicity. Untangling the debris in the South is crucial to an understanding of the Cetus stream, as well as the Sgr.

This is the first of two observational papers in which we report new insights into the formation of the Sgr stream and its neighbouring stellar halo substructures. In a companion paper, we use the multi-epoch observations of Sgr stars in Stripe 82 to measure the proper motion of the stream (cf. Carlin et al. 2012). Here, we revisit the photometric data previously available from the Sloan Digital Sky Survey (SDSS) (Fukugita et al. 1996; Gunn et

¹ Institute of Astronomy, Madingley Road, Cambridge CB3 0HA, UK

² Sternberg Astronomical Institute, Moscow State University, Universitetskii pr. 13, Moscow 119991, Russia

³ Sydney Institute for Astronomy, School of Physics, A28, The University of Sydney, NSW 2006, Australia

⁴ Kavli Institute for Astronomy and Astrophysics, Peking University, Beijing 100871, China; National Astronomical Observatories, Chinese Academy of Sciences, Beijing 100012, China

⁵ Apache Point Observatory, Sunspot, NM, 88349, USA

⁶ Department of Astronomy and Astrophysics, The Pennsylvania State University, 525 Davey Laboratory, University Park, PA 16802, USA

⁷ Department of Physics & Astronomy, The Johns Hopkins University, 3900 N. Charles Street, Baltimore, MD 21218, USA

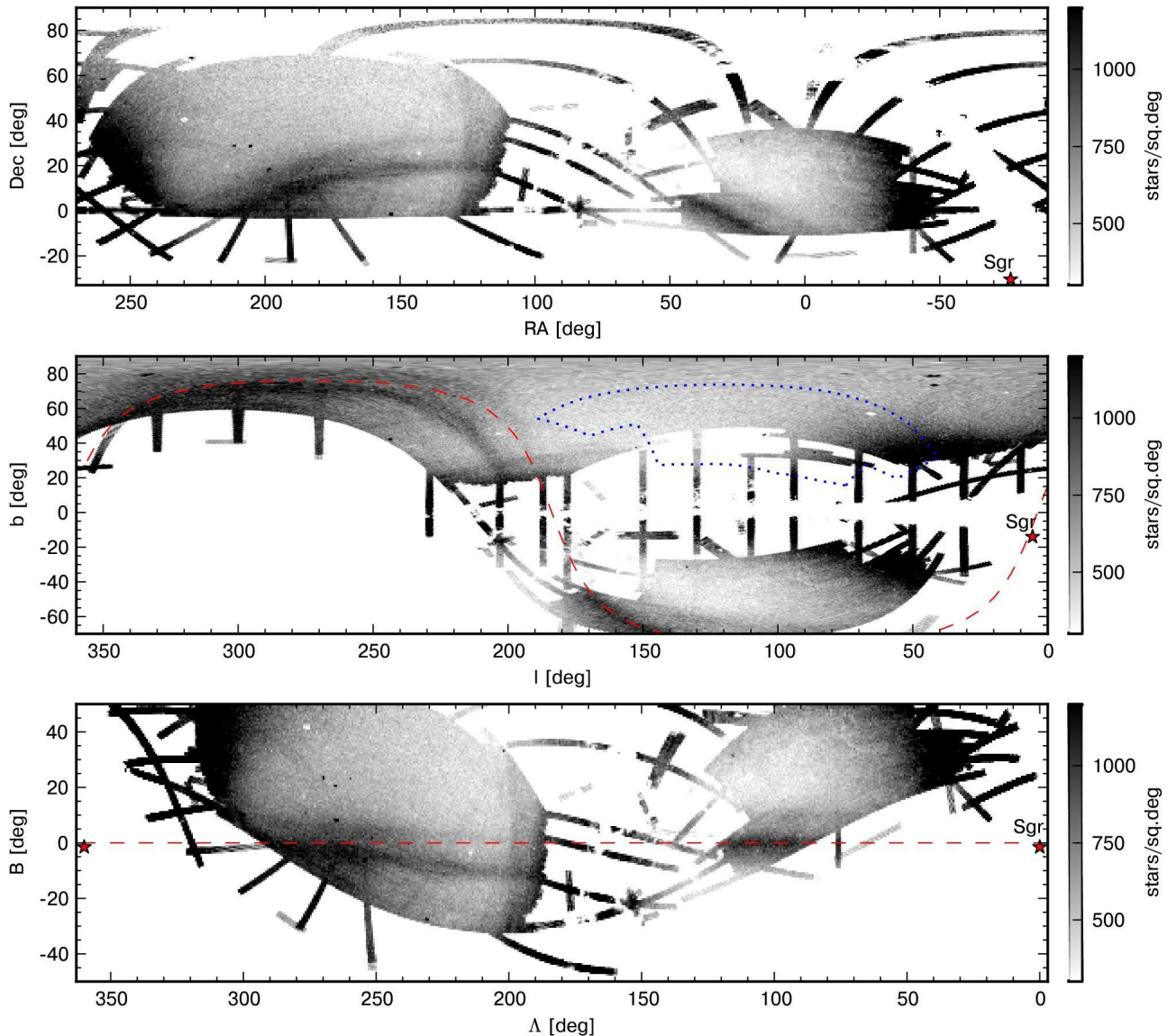


FIG. 1.— Density of MSTO stars with $0 < g-i < 0.7$ and $19.5 < i < 22$ from the SDSS DR8 on the sky in different coordinate systems. The top panel shows the map in right ascension and declination, the middle panel in Galactic coordinates, while the bottom in a coordinate system (Λ, B) aligned with the orbit of Sagittarius, as defined in Majewski et al. (2003). Several stellar streams are clearly visible, the most prominent of which is the one originating from the Sgr dSph. The Sgr stream dominating the area around North Galactic Cap has been seen in the previous SDSS data releases. While some pieces of the southern stream have been revealed before, the new data gives a much more complete picture. Similarly to the tail in the North, the tail in the South appears to have a fainter extension at one side (at higher B). The present location of Sgr dwarf is marked by a red star. The dashed red line is the projection of the Sgr orbital plane, as defined in Majewski et al. (2003), and the blue dotted line shows the outline of the comparison field as discussed in the text.

al. 1998, 2006; York et al. 2000) archives as well as new measurements made public as part of the new Data Release 8 (DR8) (Aihara et al. 2011; Eisenstein et al. 2011). Crucially, this dataset now includes significant coverage of the southern Galactic hemisphere not available to Belokurov et al. (2006).

The paper is arranged as follows. We extend the ‘Field of Streams’ plot (Belokurov et al. 2006) to the south in Section 2. This shows immediately that the Sgr stream – in the somewhat misleading nomenclature of our earlier paper – is bifurcated. Everywhere we look, in both the south and the north, there is evidence for what appears to be two streams. In Section 3, we use starcounts and Hess diagrams (Hess 1924) to characterise the density profiles and stellar populations of the streams. Where

the streams cross Stripe 82, we can take advantage of the coadded photometry (Annis et al. 2011), which reaches ~ 2 magnitudes deeper than the single epoch SDSS measurements. We use photometric metallicities to demonstrate that the two streams have different chemical properties. Untangling the substructure is considerably complicated by the existence of a further stream, already noticed by Newberg et al. (2009) and dubbed the Cetus stream. This is studied in Section 4 using blue straggler (BS) and blue horizontal branch (BHBs) stars.

2. THE STELLAR HALO IN THE SOUTH

To study substructure in the Galactic stellar halo, we select old and moderately metal-poor stars with the simple color and magnitude cuts $0 < g - i < 0.7$ and

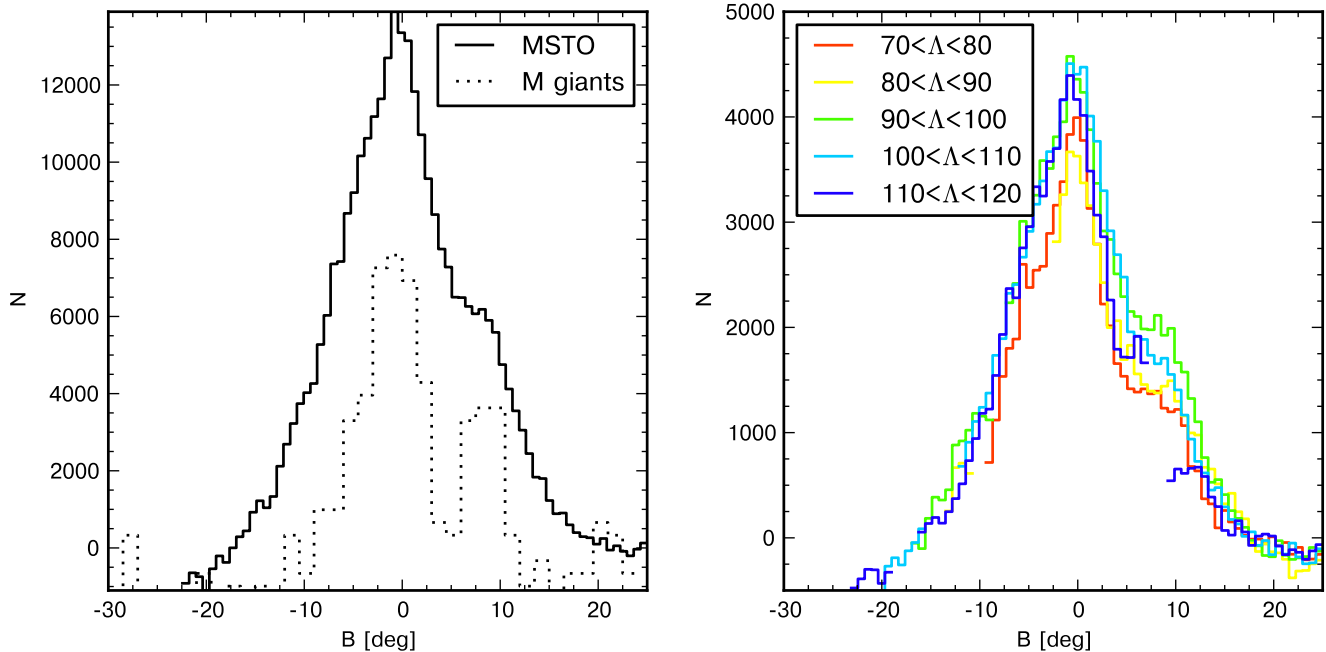


FIG. 2.— Left: Density of MSTO stars (with the same color-magnitude selection as for Figure 1) across the Sgr stream in the south ($90^\circ < \Lambda < 120^\circ$) (solid line) and the density of 2MASS M giants in the same region (dotted line). A constant background (around 7000 stars per bin) has been subtracted from the histograms. Right panel: The density of MSTO stars in different slices across the stream from $70^\circ < \Lambda < 80^\circ$ to $110^\circ < \Lambda < 120^\circ$. Although the secondary stream seems to have the same offset from the main stream at different Λ , this is not actually the case as shown in Figure 3.

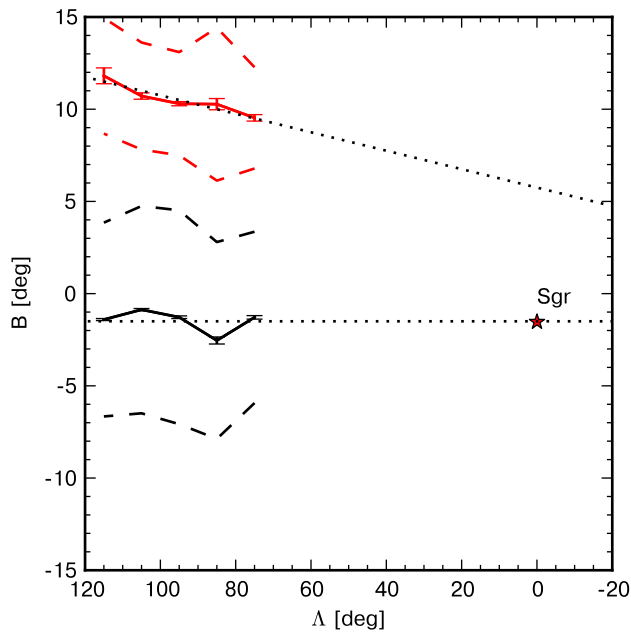


FIG. 3.— Full lines show the centers of the bright and faint streams as a function of longitude Λ as determined by a double Gaussian fit to the profile of Figure 2. The dashed lines show the 1σ widths of the streams, whilst the dotted lines show the extrapolation of the streams' centroids on approach to the Sgr remnant, which is marked by the red star.

$19.5 < i < 22$. According to model isochrones, (e.g., Girardi et al. 2004), our sample is dominated by the Main Sequence turn-off (MSTO) stars with metallicity

TABLE 1
LOCATIONS AND WIDTHS OF THE STREAMS

Λ deg	$B_{cen,bright}$ deg	$B_{cen,faint}$ deg	W_{bright} deg	W_{faint} deg
75	-1.3	9.5	4.6	2.7
85	-2.5	10.3	5.3	4.1
95	-1.3	10.3	5.8	2.8
105	-0.9	10.7	5.6	2.9
115	-1.4	11.8	5.3	3.1

TABLE 2
DISTANCES TO THE BRIGHT
STREAM

Λ deg	$m - M$ mag	$\sigma(m - M)$ mag
92.5	16.69	0.06
97.5	16.72	0.06
102.5	16.86	0.04
107.5	17.01	0.07
112.5	17.17	0.09
117.5	17.31	0.06
122.5	17.27	0.05
127.5	17.28	0.10

$Z \lesssim 0.02$ and absolute magnitude $3 \lesssim M_i \lesssim 6$, occupying the range of heliocentric distances $10 \lesssim D(\text{kpc}) \lesssim 60$.

The density of $\sim 13,000,000$ stars that passed the above color and magnitude cuts in the SDSS DR8 dataset is shown in Figure 1 in equatorial and Galactic coordinates as well as in the coordinate system approximately aligned with Sgr orbit. The arc of the Sgr tail – note the two distinct streams, or branches A and B in the notation of Be-

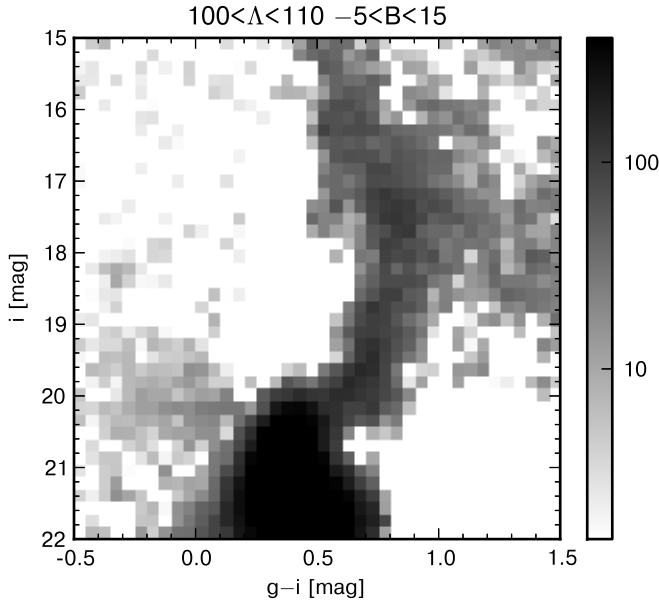


FIG. 4.— Background subtracted Hess diagram of the Sgr stream in the area defined by $100^\circ < \Lambda < 110^\circ$ and $-5^\circ < B < 15^\circ$. The background has been obtained from the symmetric area relative to the Galactic plane (which is marked by the blue dotted lines in Figure 1). Multiple stellar evolutionary phases are clearly seen: MSTO, subgiants, red giant branch, blue stragglers and BHBs at $i \sim 18.2$. The curvy black region at bright magnitudes ($i \lesssim 19$, $g - i \gtrsim 0.5$) is caused by the imperfections of the background subtraction. On top of that problematic region, the red clump is located ($i \sim 17.5$).

lokurov et al. (2006) – is clearly visible in the area around the North Galactic Cap (NGC), as has been seen in the previous SDSS data releases. Also visible in the north are the Orphan Stream and the Monoceros structure crossing the branches of the Sgr. DR8 reveals a large continuous portion of the Sgr tail in the Southern Galactic hemisphere. Curiously, this tail too is seemingly accompanied by another fainter stream following it at slightly higher declination. In fact this is not the first sighting of this structure. Watkins et al. (2009) showed that the density slice through the Sgr stream in the southern Stripe 82 contains at least two maxima.

It is useful to define a heliocentric coordinate system aligned with the Sgr stream. Such coordinate systems, whose equator aligns with the stream, have already proved useful in similar studies (e.g. Majewski et al. 2003; Koposov et al. 2010). Using the notation of Majewski et al. (2003), we introduce coordinates (Λ, B) given by their eqn (9). The equator of this spherical coordinate system coincides with the Sgr debris midplane. The bottom panel of Figure 1 shows the data in this coordinate system, with the Sgr debris now straddling the equator. This reveals that, in the new projection, rather than a “bifurcation” of the Sgr stream (the somewhat misleading term introduced in Belokurov et al. 2006), the stellar density appears resolved into two, sometimes superposed, independent streams with seemingly different angular widths and density profiles.

We are led to the conclusion that everywhere where the Sgr tidal debris can be detected in SDSS there exists at

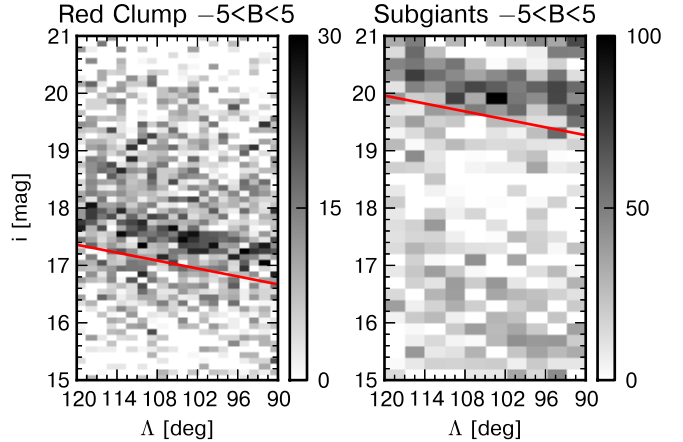


FIG. 5.— Measurement of distances and distance gradients along the stream using two different tracers: sub-giant branch stars and red clump stars. Left: 2D-histogram of red clump star counts as a function of longitude along the stream Λ and i -band magnitude. The distance gradient is clearly visible. Right: similar 2D-histogram for sub-giant stars, selected using a combination of $g-i$ and $g-r$ colors. The exact same gradient as for the red clump is clearly visible. The red line on both panels shows the distance gradient of $0.023 \text{ mag deg}^{-1}$ (offset for clarity).

least one additional density component following or overlapping the Sgr stream. In what follows, we will attempt to empirically describe and untangle these structures by examining their density profiles, distances and chemical abundances.

3. THE SGR STREAM IN THE SOUTH

3.1. Starcounts

We begin by quantifying the difference in the centroids, widths and density profiles of the streams visible in the South Galactic Region. The left panel of Figure 2 shows the density of MSTO stars across the stream in the region ($90^\circ < \Lambda < 120^\circ$). For comparison, we also show the density of M giants extracted from the 2 Micron All-Sky Survey (2MASS, see e.g., Majewski et al. 2003) using the cuts from Majewski et al. (2003), namely $J - K_s > 0.85$, $0.22 < J - H - 0.561(J - K_s) < 0.36$, $10 < K_s < 12$. Both profiles show clear evidence for bimodality, though it is unclear whether the two structures are distinct or overlapping. The right panel of Figure 2 shows cross-sections across the stream in different slices. As we march along the stream, at least in the region $90^\circ < \Lambda < 120^\circ$, the cross-section remains quite invariant, but the offset of the secondary stream from the main stream changes gently with longitude.

Let us assume that the one-dimensional profile of each stream is a Gaussian whose centroid and full width at half maximum may vary with longitude. This simple model of the stellar density in a tidal stream is of course not completely physical, but nevertheless should be sufficient to describe the pieces of the streams in the south. We now extract the centroids and widths by fitting two Gaussians to the starcount data. Figure 3 shows their behavior as a function of longitude Λ along the stream. Perhaps unsurprisingly, the tracks of the centers of two streams are not exactly parallel, but they are slightly converging. Nonetheless, it is surprising that the conver-

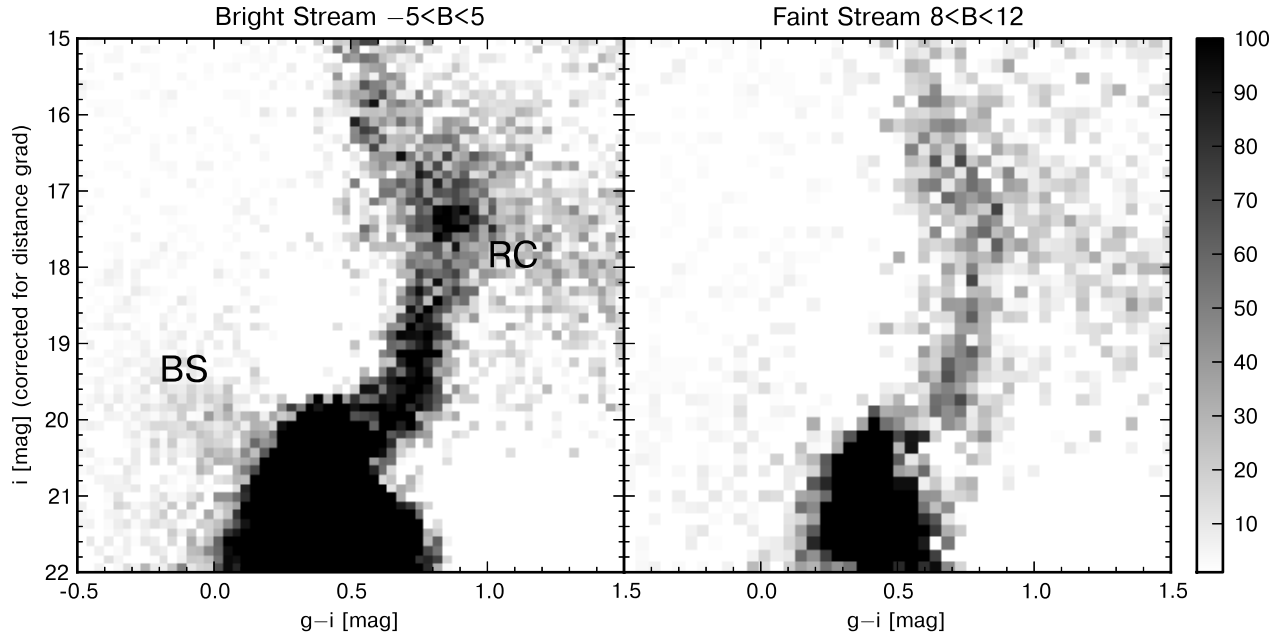


FIG. 6.— Hess diagrams determined separately for the main Southern ($-5^\circ < B < 5^\circ$) and the secondary Southern streams ($8^\circ < B < 12^\circ$). In both cases, the Hess diagrams are corrected for the distance gradient of $0.023 \text{ mag deg}^{-1}$. We have marked the red clump (RC) and blue straggler (BS) populations apparent in the brighter of the streams.

gence point is not close to the Sgr remnant (marked as a red star). This gap decrease along the stream is already a broad hint that the the two structures seen in Figure 2 are separate streams following similar but slightly different orbital paths, as opposed to a single stream with substructure. In Table 1 we provide the data on the centroids of the streams used for Figure 2.

Although Belokurov et al. (2006) used the term “bifurcation” to describe the Sgr stream in the north, the new data and analysis suggests that the term is misleading – rather, in both the north and the south, the stellar density appears to be resolved into two independent streams with different angular widths.

Of course, we have made the assumption that the profiles are Gaussian. There is evidence from simulations that stream profiles can be lop-sided (Law & Majewski 2010a). With the current data, it is not possible to distinguish with absolute certainty between the hypotheses of two streams and a single lopsided stream. Nonetheless, in our opinion, the presence of two peaks in the M giants, the detailed shape of the MSTO density profile and the behavior of centroids argues in favour of the hypothesis of two streams.

3.2. Color Magnitude Diagrams and Distance Gradients

Distances to many different parts of the Sgr stream have been measured in the past using various stellar tracers: Carbon stars (e.g. Totten & Irwin 1998), BHBs (e.g. Yanny et al. 2000; Newberg et al. 2003), sub-giant branch stars (e.g. Belokurov et al. 2006), red-clump stars (e.g. Correnti et al. 2010) and RR Lyrae variables (e.g. Prior et al. 2009; Watkins et al. 2009). However, when combined to provide as continuous a coverage of the stream as possible, the results of these methods do not always

appear to be fully consistent. Distances to the stream in the south still rely on the comprehensive study of M giants extracted from the 2MASS dataset (e.g. Majewski et al. 2003).

Here, we will rely on the SDSS photometric data and concentrate on the area in the Southern Galactic hemisphere where the stream is imaged contiguously. Our aim is to construct clean Hess diagrams of the two streams so as to analyse their stellar populations. Distances, or more accurately, relative distances along the stream are needed. If uncorrected for distance gradients, the features in our Hess diagrams lose sharpness. Here, we will use red clump and subgiant stars as distance indicators.

To construct the Hess diagrams, we make use of the fact that the Galaxy is, to a good approximation, symmetric about the Galactic plane. The blue dotted line in Figure 1 outlines the area in the North corresponding to the main patch of Southern SDSS data mirrored in the Galactic plane. In Figure 4, we show the Hess diagram of the Sgr streams in the range $100^\circ < \Lambda < 110^\circ$ and $-5^\circ < B < 15^\circ$. We have subtracted the equivalent mirrored patch as a proxy for the background region. The existence of multiple stellar populations is immediately apparent from the richness and thickness of the features in the Hess diagram. We can identify a fattened MSTO, subgiant and red giant branches, as well as populations of BHBs and BSs. Nonetheless, our background subtraction is not perfect and is the cause of some graininess in the figure, especially at brighter magnitudes. This is particularly troublesome in the region of the red clump stars.

Some of the blurring and thickening of features is of course due to the fact that the heliocentric distance is changing along the streams. Our next step is to measure the distance gradient, which we quantify by studying two

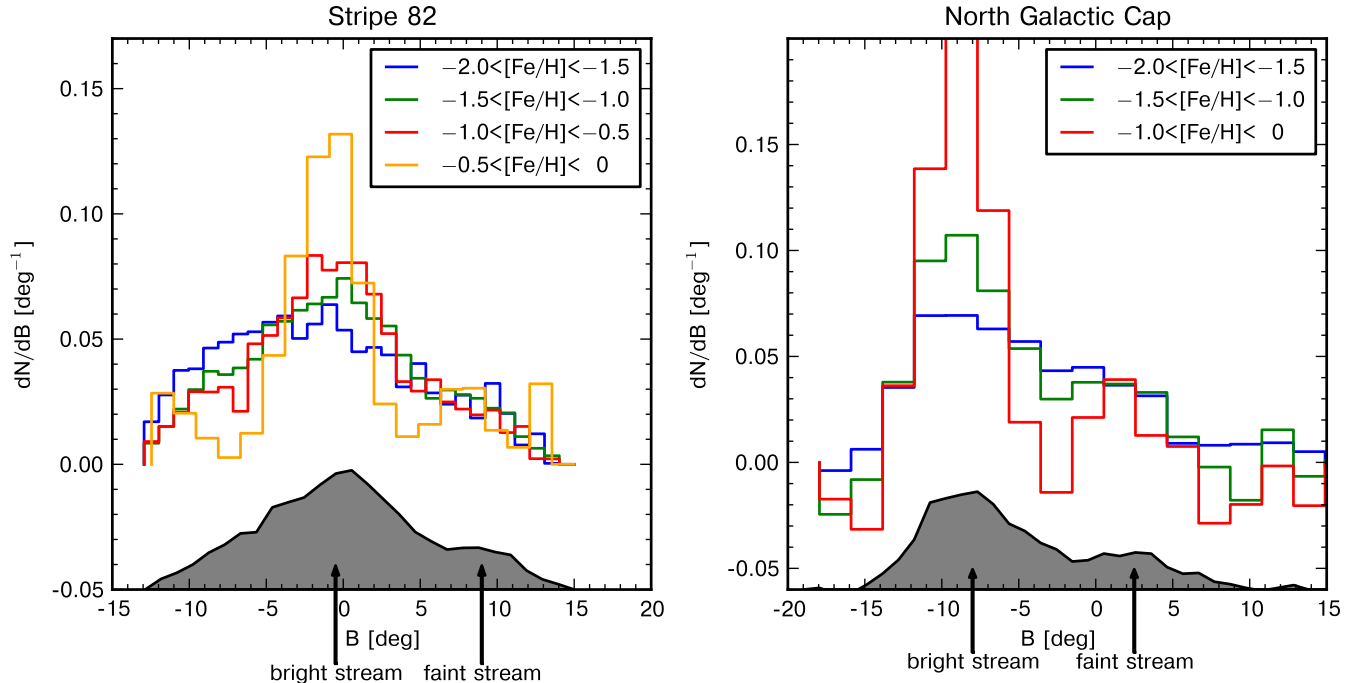


FIG. 7.— Background-subtracted distributions of stars of different metallicities across the streams. In the left panel, the stars have been selected from the Stripe 82 coadded dataset, and in the right panel from the ‘Field of Streams’ ($205^\circ < \Lambda < 240^\circ$). The shaded histograms show the density distribution of all MS stars without splitting in metallicity bins. Note that the two streams have different metallicity distribution functions, with the brighter stream containing substantial numbers of metal-rich stars as compared to the fainter stream. This is true both for the streams in the south, and those in the north. The metallicities have been measured using the formula from Bond et al. (2010).

different tracer populations in Figure 4. We select red clump stars by the colour cut (cf. Correnti et al. 2010)

$$0.8 < g-i < 0.95. \quad (1)$$

With a little more effort, we can select subgiant stars using the a linear combination of $g-i$ and $g-r$ colors, namely

$$0.45 < 0.628(g-i) + 0.529(g-r) - 0.028 < 0.55. \quad (2)$$

For both populations, we show 2D histograms of i band magnitude versus longitude along the stream Λ in Figure 5. We see that the gradient is linear to an excellent approximation, and reassuringly the same for both populations. In this area of sky, the longitudinal gradient is ~ 0.023 mag deg^{-1} . The distances measured along the brighter stream from the the red clump population are shown in the Table 2 under the assumption that $M_i = 0.6$ (Bellazzini et al. 2006).

Having identified the relative distances of populations along the stream, we can correct for the gradient and obtain cleaner Hess diagrams, as shown in Figure 6. Here, the left panel refers to the brighter stream ($-5^\circ < B < 5^\circ$), while the right panel to the fainter stream ($8^\circ < B < 12^\circ$). It is noticeable that the Hess diagram of the fainter stream shows much thinner sub-giant and red-branch regions. Furthermore, it does not possess multiple turn-offs and a prominent red-clump like the brighter southern stream. To check that the latter is not an artefact caused by low number statistics in the faint stream, we modelled the ratio of red clump to MSTO stars using a decomposition of the density profile into two Gaussians

(as used for Fig. 2). With 95 % confidence, this ratio in the fainter stream is smaller than that in the brighter. This suggests the existence of a simpler and more metal-poor population in the fainter stream, and more complex and more metal-rich population in the brighter stream.

We can confirm this result by making use of the Stripe 82 data. Stripe 82 has multi-band and multi-epoch imaging, which Annis et al. (2011) exploited to build a catalogue that reaches ~ 2 magnitudes deeper than the single epoch SDSS measurements. We compute photometric metallicities using the formula provided by Bond et al. (2010) and report the results in Figure 7 both for Stripe 82 (left panel) with $19 < r < 21.5$ and for the Sgr streams in the north between $205^\circ < \Lambda < 240^\circ$ with $19 < r < 21$. Since Stripe 82 crosses the Sgr streams at a significant angle, it is important to understand that the left part of the plot corresponds to the $\Lambda \sim 110^\circ$ region while the right corresponds to $\Lambda \sim 50^\circ$, which is much closer to the Sgr progenitor. Despite this limitation, Figure 7 shows clearly that the brighter stream has significant numbers of high metallicity stars, while the secondary stream has fewer.

4. THE CETUS AND SGR STREAMS

Whilst the picture so far is reasonably clear-cut, complications emerge when we study the bluer populations, particularly the BHB and BS stars. Of course, there is a long history of use of BHB stars for studying structure in the stellar halo. The stars are relatively abundant, and they occupy a narrow absolute magnitude range, which makes them valuable distance indicators. However, there

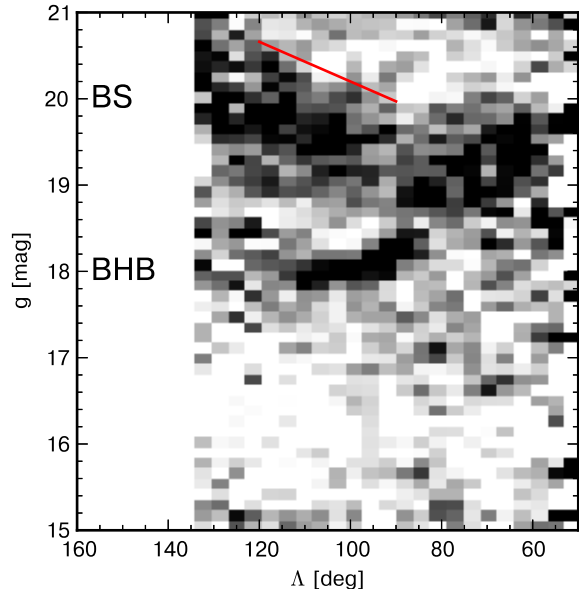


FIG. 8.— Magnitude distribution of BHB/BS-like stars as a function of the angle along the stream. The diagram shows two classes of objects coming from two structures: BS from Sgr stream with the same distance gradient as the subgiants/red clump (shown as an offset red line), and BHBs from Cetus stream with an opposite distance gradient at $g \approx 18$ and $80^\circ \lesssim \Lambda \lesssim 120^\circ$.

TABLE 3
DISTANCES TO THE CETUS STREAM

$\phi_{1,Cetus}$ deg	$m - M$ mag	$\sigma(m - M)$ mag
-17.5	17.74	0.03
-12.5	17.73	0.01
-7.5	17.65	0.02
-2.5	17.54	0.02
2.5	17.51	0.02
7.5	17.43	0.01
12.5	17.35	0.02
17.5	17.34	0.02
22.5	17.39	0.04

has been a slight confusion as to the absolute magnitude of a typical BHB star in the SDSS filter system: for example Yanny et al. (2000) and Niederste-Ostholt et al. (2010) have used $M_g = 0.7$, while Newberg et al. (2009) advocate the use of $M_g = 0.5$. It is also known that the BHB absolute magnitude is also a function of color and metallicity. Fortunately, we do not need to address this issue here, as we will mostly use relative distances.

Guided by the photometric properties of the globular cluster BHBs studied by An et al. (2008), we choose to use the following simple color cuts to select candidate BHB stars in the SDSS data: $0.9 < u - g < 1.3$, $-0.35 < g - r < 0.0$. At higher values of $g - r$, the contamination from main sequence stars increases sharply. Of course, this color selection also identifies out the BS stars (Yanny et al. 2000). We therefore might expect that the density distribution along the distance axis typically shows two enhancements corresponding to BHB and BS stars separated by ~ 2 magnitudes. Note that the BHBs have a narrow band of intrinsic luminosities and so generate

tight structures, whereas the BSs are poorer distance indicators and produce more diffuse structures (see e.g., Figure 4 of Deason et al. 2011).

Figure 8 shows the density of stars satisfying our colour cut as a function of apparent magnitude and longitude. There are indeed two evident structures present, but they do not correspond to two roughly parallel density peaks which might be naturally interpreted as BS and BHBs from the same structure. Rather the figure forces upon us the interpretation that there are two classes of objects arising from two distinct structures: the thick structure possesses the same longitudinal distance gradient as the subgiant and red clump stars, and this can be identified with BSs from the Sgr stream. The other, thinner structure has the opposite distance gradient, and we shall see that these are BHB stars lying in an entirely different structure, namely the Cetus stream.

The discovery of the Cetus stream was announced by Newberg et al. (2009). They noticed a stream-like overdensity in low metallicity stars in SDSS DR7 that crosses the Sgr stream in the south at $b \sim -70^\circ$. The Cetus stream can be distinguished from the Sgr on the basis of its markedly lower ratio of BS to BHB stars and its different kinematics. They also suggested that some BHB stars previously attributed to the Sgr stream instead properly belong to the Cetus stream.

In the middle panel of Figure 9, we display the density distribution of stars on the sky satisfying the color cuts $-0.3 < g - r < 0$ and $0.9 < u - g < 1.35$ together with $18.5 < g < 20$. The magnitude cut ensures that these stars are primarily BSs, and they do indeed align with the Sgr stream along $B \approx 0^\circ$ (following the MSTO distribution showed on the left panel of Figure 9). There is, however, some patchiness in the stellar distribution; this seems to be associated with granularity in the extinction. We show the extinction map of Schlegel et al. (1998) in the right panel of Figure 9, and there is indeed an anomalous patch of high extinction along the path of the stream at $\Lambda \approx 85^\circ$, $B \approx 5^\circ$.

The spatial distribution of the Cetus stars in Figure 8 is not easy to understand as the coordinate system is aligned with the Sgr orbit. To reconstruct the orientation of Cetus, we first select the BHBs in the range $17 < g < 18.5$ and $80^\circ < \Lambda < 130^\circ$ and $-5^\circ < B < 30^\circ$. We find the direction of the stream by fitting a Gaussian to their magnitudes, allowing the center of the Gaussian to vary linearly with Λ and B . The fit yields the magnitude of the BHBs as

$$g = -0.0112(\Lambda - 100) - 0.0064B + 18.08. \quad (3)$$

together with the width of the Gaussian as 0.1 mag. This allows us to refine our selection of Cetus candidate members, as shown in the left panel of Figure 10. The arrow shows our measured distance gradient of Cetus BHBs, which should lie roughly along the extension of the stream. Despite low number statistics, the stream is clearly visible and is at significant angle to the Sgr stream. To confirm the orientation of the stream, the middle panel shows the distance modulus of BHBs as a function of angular distance along the Cetus stream. This angular distance has been derived as longitude in the rotated coordinate system with the pole at $(\alpha_p, \delta_p) = (294^\circ, 30^\circ)$ and longitude zero-point at $\alpha_0 = 25^\circ$. The absolute magnitudes of BHBs have been derived from

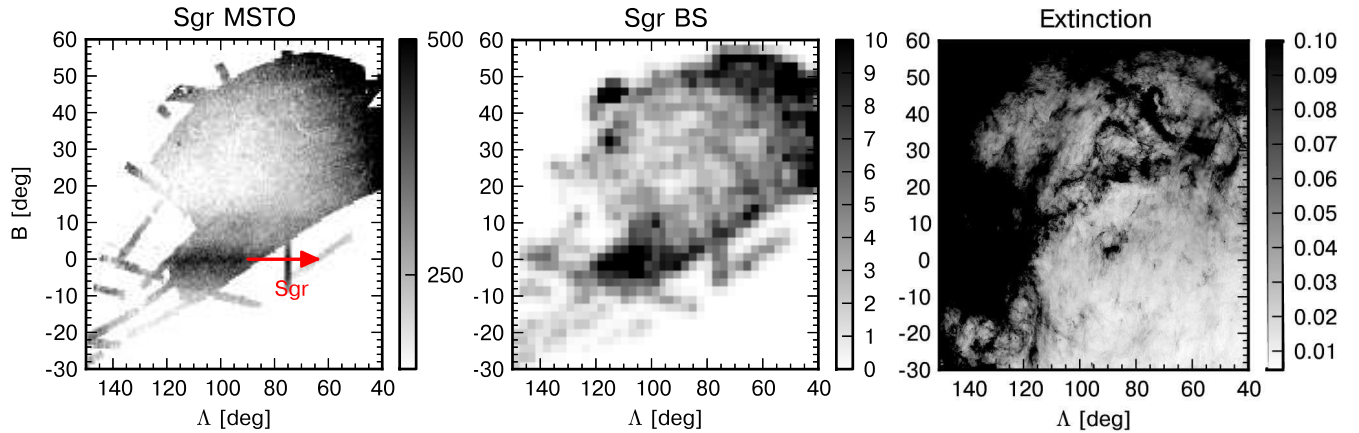


FIG. 9.— Left: Density of high Galactic latitude ($|b| > 20^\circ$) MSTO stars selected using the same color-magnitude cuts as for Figure 1. The arrow shows the direction of motion of Sgr stars. Middle: Density of high Galactic latitude BS stars $-0.3 < g-r < 0$, $0.9 < u < 1.3$ and $18.5 < g < 20$ on the sky confirming their attribution to the Sgr streams. The 1-D profile of the BS stars across the stream confirms that the BS stars are present in the secondary stream too (not shown). The slight dip in the density map visible at $\Lambda \sim 85^\circ$ $B \sim 5^\circ$ is caused by problems with the extinction correction. The peak at $\Lambda \sim 110^\circ$ $B \sim 30^\circ$ is associated with M33. Milky way disk stars are also visible at lower latitudes. Right: Schlegel et al. (1998) extinction map for this region with the elevated extinction ($E(B-V) \sim 0.1$) patch at $\Lambda \sim 85^\circ$ $B \sim 5^\circ$.

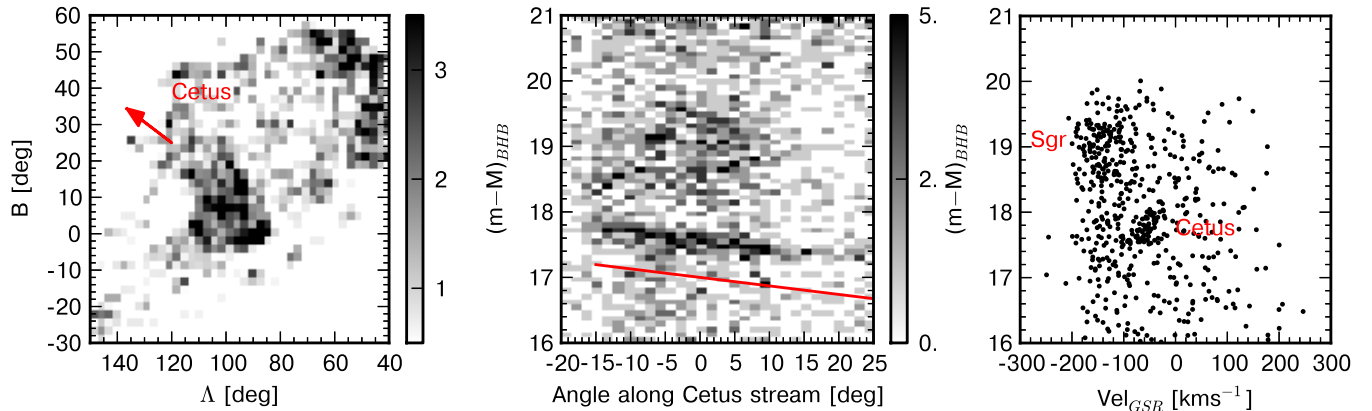


FIG. 10.— Left: Density of Cetus stream BHB stars on the sky. The stars were selected to be BHB-like according to standard $g-r$, $u-g$ cuts, Galactic latitude cut ($|b| > 20^\circ$), together with a position-dependant distance cut selecting predominantly Cetus stream stars. The arrow shows our measured distance gradient of Cetus stream BHBs. Middle: BHB stars in a coordinate system aligned with the Cetus stream, which is now clearly visible as an extended, narrow structure. The red line shows the distance gradient of $0.013 \text{ mag deg}^{-1}$ offset for clarity. Right: The kinematical separation of the BS+BHB stars belonging to Sgr and Cetus stream for $80^\circ < \Lambda < 120^\circ$ and $-10^\circ < B < 20^\circ$. The velocity of Cetus stream stars in the Galactic rest frame is between -100 and -50 km s^{-1} , while Sgr stars have velocities between -200 and -100 km s^{-1} .

$g-r$ colors using Eq. 7 of Deason et al. (2011). A narrow structure is visible spanning at least 40° . The measurement of these distances along the structure is given in Table 3. We can further strengthen the case that most of the BHB stars belong to the Cetus stream by studying their kinematics. The right panel of Figure 10 shows the BS and BHB stars with well measured velocities ($\sigma_V < 30 \text{ km s}^{-1}$) and $-15^\circ < B < 30^\circ$, $80^\circ < \Lambda < 120^\circ$). The velocity of Cetus stars corrected for Galactic rotation, V_{GSR} ⁸ is between -100 and -50 km s^{-1} while Sgr stars have velocities between -200 and -100 km s^{-1} (cf., Newberg et al. 2009). There is a clear and clean kinematical separation of the BS and BHB stars belonging to Sgr and Cetus. Given the distance gradient and radial velocity of

Cetus, we see that its orbital motion is counter-rotating with respect to that of Sgr.

5. CONCLUSIONS

We have studied the Sagittarius (Sgr) stream in the southern Galactic hemisphere. In the SDSS Data Release 8, at most locations along the orbit, an additional stream component can be discerned. As evidenced from the density profiles of main sequence turn-off stars and M giants, as well as the tracks of the components on the sky (see Fig. 2), we think that the most natural interpretation is that there are two streams. Our modelling of the cross-sections of the density suggests the existence of a thicker brighter stream and a thinner fainter stream, offset by $\sim 10^\circ$. The streams differ in integrated luminosity by a factor of 5–10. There is also strong evidence that the two streams have different metallicity distribution functions.

⁸ This assumes a Galactic rotation velocity of 236 km s^{-1} (Bovy et al. 2009), while the Sun's peculiar velocity is taken from Coşkunoglu et al. (2011)

We used red clump and subgiant stars to measure the distance gradients along the streams. This enables us to construct composite Hess diagrams to study the stellar populations in the streams. The brighter stream shows evidence for multiple turn-offs and a prominent red clump, whereas the secondary stream does not. This suggests that the brighter stream is composed of more than one stellar population, and contains a significant number of metal-rich stars, much like the Sgr remnant itself. By contrast, the fainter stream is dominated by a metal-poor population. This conclusion is also supported by our photometric metallicities computed for the region where the Sgr streams cross the ultra-deep SDSS Stripe 82 coadded data.

Our analysis of the new data allows us to untangle a complicated mix of tidal debris around the South Galactic Cap, where the Sgr streams are crossed by the Cetus Stream at an angle of $\sim 30^\circ$. The Sgr and Cetus streams have similar distances, though their stellar populations and kinematics are different. The structures are not part of the same disruption event, as the Cetus stream is counterrotating with respect to the Sgr. On the basis of their density distribution and kinematics, we have shown that most of the BSs belong to the Sgr stream, whereas most of the BHBs belong to the Cetus Stream, in this part of the sky. The BS to BHB ratio in the two streams is strikingly different, as already pointed out by Newberg et al. (2009). Good spectroscopic coverage of the area is essential to disentangle the multiple overlapping streams with different chemical properties, following different distance gradients.

The work in this paper has extended the ‘Field of Streams’ (Belokurov et al. 2006) to the south. The new imaging data show that, just as in the north, the Sgr stream is accompanied by a fainter stream. The right-hand panel in Fig 7 shows that the population mix in the fainter stream of the “bifurcation” around the North Galactic Cap does not contain as many metal-rich stars as the brighter stream. The simplest explanation is that the southern faint stream is part of the same structure as the northern faint stream.

These results raise the question: Is it possible to produce the streams with the properties described in this paper in a disruption of one galaxy or is more than one progenitor necessary?

Recently, two possible scenarios, both in context of the Sgr dSph disruption, have shown how to form two almost parallel tidal streams from the debris of one parent galaxy. Although Fellhauer et al. (2006) did not fully match the available data, they did suggest that branches A and B (see Belokurov et al. 2006) could be reproduced by multiple wraps of the same stream offset on the plane of the sky by small amount of differential precession. In this picture, the fainter stream in the North Galactic Cap area corresponds to the dynamically old tidal debris in the Sgr trailing arm. However, this mechanism does not produce two distinct streams in the south and now seems to be ruled out.

Alternatively, Peñarrubia et al. (2010) point out that if the Sgr progenitor had a rotating stellar disk misaligned with respect to its orbit, then stripping naturally produces bifurcated debris tracks on the sky. However, the

model seems to be ruled out as it has been difficult to find strong evidence for residual rotation in the remnant of the Sgr dwarf (Peñarrubia et al. 2011). Moreover, in the scenario of Peñarrubia et al. (2010) the two streams are not expected to differ significantly in their stellar populations content. This prediction is somewhat difficult to reconcile with the new data on the stellar populations of the streams. In some other models although, such as Law & Majewski (2010a) the streams that form at consecutive pericentric passages could have somewhat different metallicity distributions, as metal-rich stars could have been torn predominantly later, from deeper within the gravitational potential of the satellite.

Finally, it is tempting to suggest that the two streams with different properties have actually originated from two different progenitors. The infall of satellites in groups is not particular but general, as best illustrated by the recent arrival of the Large and Small Magellanic Clouds. Cosmological simulations of structure formation also find plenty of evidence for group infall (e.g. Li & Helmi 2008). The picture painted by the data looks more complex than this and remains a challenge to understand. Although there has been substantial progress in modelling the Sgr (see e.g., Fellhauer et al. 2006; Peñarrubia et al. 2010; Law & Majewski 2010a), it remains true that there is no explanation of the nature of the two Sgr streams.

SK acknowledges financial support from the Science and Technology Funding Council of the United Kingdom, whilst VB and MG thanks the Royal Society for the award of a University Research Fellowship. GFL thanks the Australian Research Council for support through his Future Fellowship (FT100100268) and Discovery project (DP110100678). Most of the data processing has been done using the python programming language and the following open source modules: numpy⁹, scipy¹⁰, matplotlib¹¹. The SDSS data was accessed using local SDSS copy stored in PostgreSQL database and Q3C module (Koposov & Bartunov 2006). Funding for SDSS-III has been provided by the Alfred P. Sloan Foundation, the Participating Institutions, the National Science Foundation, and the U.S. Department of Energy Office of Science. The SDSS-III web site is <http://www.sdss3.org/>.

SDSS-III is managed by the Astrophysical Research Consortium for the Participating Institutions of the SDSS-III Collaboration including the University of Arizona, the Brazilian Participation Group, Brookhaven National Laboratory, University of Cambridge, University of Florida, the French Participation Group, the German Participation Group, the Instituto de Astrofísica de Canarias, the Michigan State/Notre Dame/JINA Participation Group, Johns Hopkins University, Lawrence Berkeley National Laboratory, Max Planck Institute for Astrophysics, New Mexico State University, New York University, Ohio State University, Pennsylvania State University, University of Portsmouth, Princeton University, the Spanish Participation Group, University of Tokyo, University of Utah, Vanderbilt University, University of Virginia, University of Washington, and Yale University.

⁹ <http://numpy.scipy.org>

¹⁰ <http://www.scipy.org>

REFERENCES

- Aihara, H., Allende Prieto, C., An, D., et al. 2011, *ApJS*, 193, 29
- An, D., Johnson, J. A., Clem, J. L., et al. 2008, *ApJS*, 179, 326
- Annis, J., Soares-Santos, M., Strauss, M. A., et al. 2011, arXiv:1111.6619
- Bellazzini, M., Newberg, H. J., Correnti, M., Ferraro, F. R., & Monaco, L. 2006, *A&A*, 457, L21
- Belokurov, V., Zucker, D. B., Evans, N. W., et al. 2006, *ApJ*, 642, L137
- Bond, N. A., Ivezić, Ž., Sesar, B., et al. 2010, *ApJ*, 716, 1
- Bovy, J., Hogg, D. W., & Rix, H.-W. 2009, *ApJ*, 704, 1704
- Carlin, J. L., Majewski, S. R., Casetti-Dinescu, D. I., et al. 2012, *ApJ*, 744, 25
- Chou, M.-Y., Majewski, S. R., Cunha, K., et al. 2007, *ApJ*, 670, 346
- Chou, M.-Y., Cunha, K., Majewski, S. R., et al. 2010, *ApJ*, 708, 1290
- Correnti, M., Bellazzini, M., Ibata, R. A., Ferraro, F. R., & Varghese, A. 2010, *ApJ*, 721, 329
- Coşkunoğlu, B., Ak, S., Bilir, S., et al. 2011, *MNRAS*, 412, 1237
- Deason, A. J., Belokurov, V., Evans, N. W., 2011, *MNRAS*, 416, 2903
- Eisenstein, D. J., Weinberg, D. H., Agol, E., et al. 2011, *AJ*, 142, 72
- Fellhauer, M., Belokurov, V., Evans, N. W., et al. 2006, *ApJ*, 651, 167
- Fukugita, M., Ichikawa, T., Gunn, J. E., et al. 1996, *AJ*, 111, 1748
- Girardi, L., Grebel, E. K., Odenkirchen, M., & Chiosi, C. 2004, *A&A*, 422, 205
- Gunn, J. E., Carr, M., Rockosi, C., et al. 1998, *AJ*, 116, 3040
- Gunn, J. E., Siegmund, W. A., Mannery, E. J., et al. 2006, *AJ*, 131, 2332
- Hess, R., "Die Verteilungsfunktion der absol. Helligkeiten etc.". Probleme der Astronomie. Festschrift für Hugo v. Seeliger. Springer, Berlin. p. 265.
- Ibata, R. A., Gilmore, G., & Irwin, M. J. 1994, *Nature*, 370, 194
- Johnston, K. V., Spiegel, D. N., & Hernquist, L. 1995, *ApJ*, 451, 598
- Jurić, M., Ivezić, Ž., Brooks, A., et al. 2008, *ApJ*, 673, 864
- Koposov, S., & Bartunov, O. 2006, *Astronomical Data Analysis Software and Systems XV*, 351, 735
- Koposov, S. E., Rix, H.-W., & Hogg, D. W. 2010, *ApJ*, 712, 260
- Law, D. R., & Majewski, S. R. 2010a, *ApJ*, 714, 229
- Law, D. R., & Majewski, S. R. 2010b, *ApJ*, 718, 1128
- Li, Y.-S., & Helmi, A. 2008, *MNRAS*, 385, 1365
- Lynden-Bell, D., & Lynden-Bell, R. M. 1995, *MNRAS*, 275, 429
- Majewski, S. R., Skrutskie, M. F., Weinberg, M. D., & Ostheimer, J. C. 2003, *ApJ*, 599, 1082
- Majewski, S. R., Kunkel, W. E., Law, D. R., et al. 2004, *AJ*, 128, 245
- Martínez-Delgado, D., Peñarrubia, J., Jurić, M., Alfaro, E. J., & Ivezić, Z. 2007, *ApJ*, 660, 1264
- Mateo, M., Mirabal, N., Udalski, A., et al. 1996, *ApJ*, 458, L13
- Monaco, L., Bellazzini, M., Bonifacio, P., et al. 2007, *A&A*, 464, 201
- Newberg, H. J., Yanny, B., Rockosi, C., et al. 2002, *ApJ*, 569, 245
- Newberg, H. J., Yanny, B., Grebel, E. K., et al. 2003, *ApJ*, 596, L191
- Newberg, H. J., Yanny, B., & Willett, B. A. 2009, *ApJ*, 700, L61
- Niederste-Ostholt, M., Belokurov, V., Evans, N. W., & Peñarrubia, J. 2010, *ApJ*, 712, 516
- Peñarrubia, J., Belokurov, V., Evans, N. W., et al. 2010, *MNRAS*, 408, L26
- Peñarrubia, J., Zucker, D. B., Irwin, M. J., et al. 2011, *ApJ*, 727, L2
- Prior, S. L., Da Costa, G. S., & Keller, S. C. 2009, *ApJ*, 704, 1327
- Schlegel, D. J., Finkbeiner, D. P., & Davis, M. 1998, *ApJ*, 500, 525
- Totten, E. J., & Irwin, M. J. 1998, *MNRAS*, 294, 1
- Watkins, L. L., Evans, N. W., Belokurov, V., et al. 2009, *MNRAS*, 398, 1757
- Yanny, B., Newberg, H. J., Kent, S., et al. 2000, *ApJ*, 540, 825
- Yanny, B., Newberg, H. J., Johnson, J. A., et al. 2009, *ApJ*, 700, 1282
- York, D. G., Adelman, J., Anderson, J. E., Jr., et al. 2000, *AJ*, 120, 1579

¹¹ <http://matplotlib.sf.net>